Utilizing vapor swelling of surface-initiated polymer brushes to develop quantitative measurements of brush thermodynamics and grafting density

Sara V. Orski [1], Richard J. Sheridan [1], Edwin P. Chan, Kathryn L. Beers[*]

Materials Science and Engineering Division, The National Institute of Standards and Technology (NIST)[2] Gaithersburg, MD, USA

ABSTRACT

The stimuli-responsive behavior of densely grafted polymer brushes makes them attractive for designing tunable coatings and thin film sensors, provided physical properties and thermodynamics of the brush are well characterized. This work investigates the swelling of highly extended poly(methyl methacrylate) polymer brushes in solvent vapors. All brushes have identical grafting density, but differing degrees of polymerization. Brushes were equilibrated in various saturated vapors, then characterized by X-ray reflectivity to measure thickness and scattering length density. One dimensional swelling normal to the surface is observed for all brush—solvent pairs; brushes swollen in good solvents generally exhibit decreasing polymer density along the thickness direction of the brush, while poor solvents swell the brush with minimal changes in the bulk brush density profiles relative to the dry state. Comparison of changes in brush height and film density upon swelling to existing mean-field models indicate that vapor solvation thermodynamics of polymer brush thin films is not explained by existing theory.

Published by Elsevier Ltd.

1. Introduction

Polymer brushes exhibit fundamentally different physical properties relative to their thin film analogs resulting from the highly extended, non-overlapping chain configuration within brushes, where the distance between end-tethered brush anchor points is much less than twice the radius of gyration of the free polymer (d << $2R_g$) [1—4]. The morphology of polymer brushes generates thin film interfaces that are highly sensitive to small changes in environment. The presence of solvent, as a liquid or vapor, can affect thin film properties such as electrical conductivity [5], glass transition [6], or compression hysteresis [7], making polymer brushes potentially useful as advanced stimuli-responsive coatings [8—12]. However, implementing brushes as tunable thin films requires a deep understanding of the physics that control brush response.

The distinctive physical properties of polymer brushes are attributed to three interdependent thermodynamic parameters, which are the grafting density of chains (σ), the brush molecular mass, and the solvent quality. A scaling relationship, based on the Flory approximation, relates brush thickness (h) to degree of polymerization (N) and grafting density (σ) [8,13] which has been supported through several experimental and theoretical studies: [1,14—17]

$$h \propto N\sigma^n \qquad (1)$$

$$\sigma = h_d \rho N_A / M_n \qquad (2)$$

The power law exponent, n, varies depending on the grafting density and the solvation quality of the brush chains [1,18]. Generally $n = 0$ for low grafting density "brushes" formed via the grafting-to technique [14]. The brush regime is characterized by $n \approx 0.33$, but experiments have demonstrated higher power exponents for highly extended brushes [19,20]. To use equation (1), or its underlying physical model [17,21], as a quantitative structure-e—property relationship requires accurate determination of σ. Grafting density is calculated based on Equation (2), where h_d is dry brush thickness, M_n is the number average molecular mass of the polymer, N_A is Avogadro's number and ρ is the bulk density of the

* Corresponding author.
  E-mail addresses: beers@nist.gov, kathryn.beers@nist.gov (K.L. Beers).
  [1] Authors contributed equally to this work.
  [2] Official contribution of the National Institute of Standards and Technology; not subject to copyright in the United States.

polymer. Equation (2) facilitates a practical way to calculate grafting density based on the bulk density of the polymer and molecular mass [22], provided that M_n can be accurately determined. Still, this remains a challenge, since the model assumptions in equation (1) do not fully address behavior in the crossover regimes, where significant chain interactions may occur, but scaling is not well understood.

Measurement of polymer brush M_n becomes more challenging as grafting density increases because chains in the strong stretching regime often require polymer synthesis directly from the surface, where precise brush molecular mass is unknown. A soluble, small molecule initiator is often added to polymer brush syntheses, forming solution polymer that can be recovered and characterized to approximate brush M_n. Prior experiments have compared differences in solution and brush M_n, obtained by cleaving polymer from large surface area supports and comparing to sacrificial-initiated polymer [23–27]. These studies did not yield consistent results among each other, causing ambiguity in the molecular mass characterization of strongly stretched brushes.

Furthermore, recent Monte Carlo simulations have been used to investigate how surface confinement of the initiator affects monomer diffusivity to active chain ends of polymer brushes compared to equivalent bulk polymerizations [28,29]. Simulated reaction kinetics indicated that brush molecular mass decreased relative to bulk polymerization as grafting density of the brush chains increased [29]. These results suggest the molecular mass equivalency assumption may not be accurate.

An alternative approach to determining the structural components of the polymer brush, e.g., M_n and σ, utilizes direct swelling of the polymer brush instead of relying on solution polymer or polymer from cleaved substrates. This method has been previously used to stimulate and measure changes in mechanical properties [30–33] and detect zwitterionic complexes [34] within polymer brushes. In these systems, the introduction of solvent induces conformational changes of the chains and brush surface energy as the solvent content of the brush increases [12]. The swelling response of polymer brushes relies on the interdependent parameters of grafting density, molecular mass and solvent quality; therefore, measuring the brush after systematically changing one of these parameters, such as solvent quality, will elucidate what thermodynamic changes are occurring within the brush when the other two (σ and M_n) remain constant. Repeating these experiments while varying molecular weight, then grafting density will generate a phase map of the brush swelling response where the contributions of each parameter to overall brush thermodynamics are quantified. This approach then enables the measurement of one unknown parameter, such as σ, based on the degree of brush swelling. Such a technique would have broad applicability to various brush chemistries and architectures.

In the present study, we use X-ray reflectivity (XRR) to study the equilibrium swelling behavior of polymer brushes in solvent vapors of different solvent quality. Two poly(methyl methacrylate) (PMMA) brushes with the same surface initiator concentration but different thicknesses (due to different degrees of polymerization) are synthesized using atom transfer radical polymerization (ATRP). XRR is used to measure the changes in the PMMA brush thickness and polymer volume fraction at equilibrium with different solvent vapors, while grafting density of chains is constant. The density and thickness changes of the brushes are compared to determine the dimensionality of brush swelling, and experimental data are compared to a mean-field theory to attain grafting density from swelling results. Challenges in determining solvent quality and grafting density will be discussed as well as the limitations of polymer brush thermodynamics as it applies to vapor phase swelling.

2. Experimental

2.1. Materials

Silicon wafers (N-type (100) polished) were purchased from University Wafer. Toluene was purchased from Sigma Aldrich and distilled over calcium hydride prior to use. Methyl methyacrylate (MMA) was stirred over calcium hydride for 24 h and distilled to remove inhibitor. All other reagents were purchased from Sigma Aldrich and used as received. Certain commercial equipment, instruments, or materials are identified in this paper in order to specify the experimental procedure adequately. Such identification is not intended to imply recommendation or endorsement by the National Institute of Standards and Technology, nor is it intended to imply that the materials or equipment identified are necessarily the best available for the purpose.

2.2. Formation of ATRP initiator monolayers

Silicon wafers (2.5 cm × 2.5 cm) were sonicated for 10 min each in acetone, ethanol, and 18.2 MΩ nanopore deionized water in a glass staining jar, dried under a stream of nitrogen, and subjected to ultraviolet oxygen (UVO) cleaning (Jelight UVO-Cleaner Model 342) for 10 min to generate a hydrophilic surface (static contact angle < 10°). The ATRP initiator, 11-(chlorodimethylsilyl)undecyl 2-bromo-2-methylpropanoate, was synthesized according to literature procedures [35,36] and immediately used for the monolayer reaction. A 0.01 mol/L solution of the silane in dry toluene (25 mL) was added to the staining jar wells containing the silicon wafers. Triethylamine (10 μL) was added as a catalyst and acid scavenger. The jar was sealed with Teflon tape and left overnight. After 16 h, the substrates were removed, rinsed with toluene, dichloromethane, and acetone, and dried under nitrogen. The initiator layers were 1.9 nm ± 0.1 nm as measured by ellipsometry. An atomic force microscope (AFM) height image of a representative monolayer is shown in Fig. 1. The initiator had a root means square (RMS) roughness of 0.78 nm.

2.3. Surface initiated atom transfer radical polymerization (SI-ATRP) of methyl methacrylate for thin polymer brushes

SI-ATRP of the thin polymer brushes was based on a procedure by Rühe and coworkers [37]. A 50 mL septum-sealed glass reactor was set up in a 30 °C oil bath with the initiator wafer suspended on glass support above a stir bar. Methyl methacrylate (18.5 g, 184.7 mmol) and anhydrous anisole (20 mL), and ethyl α-bromoisobutyrate (26 μL, 0.18 mmol) was added to the reactor and bubbled with argon gas 60 min to remove oxygen. Simultaneously, 2 mL of acetone and N,N′,N″,N‴-pentamethylenediethylenetriamine (PMDETA, 40 μL, 0.0.19 mmol) was deoxygenated separately, as was a solution of CuBr (26 mg, 0.18 mmol) in 1 mL of anisole. PMDETA and CuBr were combined to form the solubilized copper–ligand complex and that solution was cannula transferred into the reactor. The reaction was stirred at 35 rad/s for 20 h. The reaction was quenched by opening the reactor to atmosphere and the wafer was rinsed with toluene, dichloromethane, and sonicated in dichloromethane (30 mL for 15 min) until the dry thickness measurement was consistent. The brush was annealed under vacuum at 160 °C (2.6 × 10^3 Pa) for 5 h to ensure all solvent was removed. A scheme of the reaction is available in Scheme S1 of the supporting information.

2.4. Surface initiated atom transfer radical polymerization (SI-ATRP) of methyl methacrylate for thick polymer brushes

SI-ATRP of the thick polymer brushes proceeded based on a modified procedure by Gorman et al. [38] A 50 mL septa-sealed
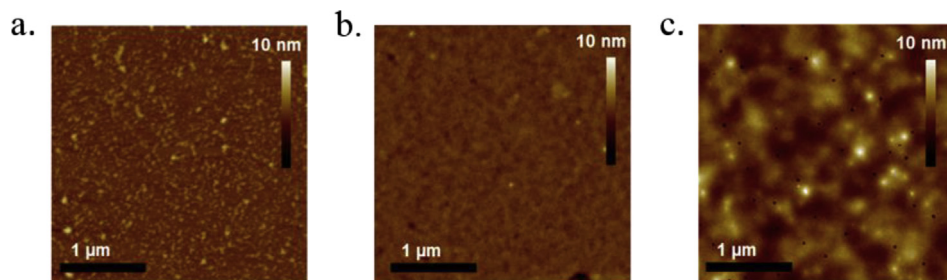
Fig. 1. AFM Height Images of ATRP initiator (a, $R_q = 0.78$ nm) and dry polymer brushes for the thin (b, $R_q = 0.4$ nm) and thick (c, $R_q = 2.0$ nm) films.

glass reactor was set up in a 30 °C oil bath with the initiator wafer suspended on glass support above a stir bar. CuCl (0.32 g, 3.2 mmol) and $CuCl_2$ (5.5 mg, 0.04 mmol) were added and the reactor was put under vacuum and backfilled with argon several times to remove oxygen. The flask remained under positive pressure with argon. In a separate flask, methyl methacrylate (17.4 g, 174.2 mmol) and 2,2'-bipyridine (1.03 g, 6.6 mmol) were dissolved in a methanol/water mixture (85:15 volume fraction) and bubbled with argon 1 h. A stock solution of ethyl α-bromoisobutyrate (100 μL, 0.68 mmol) in 1 mL of methanol was deoxygenated separately. The monomer solution was cannula transferred into the reactor and 0.1 mL of the ethyl α-bromoisobutyrate solution was added to the reactor via syringe. The reaction stirred at 35 rad/s for 16 h. The reaction was quenched by opening the reactor to atmosphere and the wafer was rinsed with toluene, dichloromethane, and sonicated in dichloromethane (30 mL for 15 min) until the dry thickness measurement was consistent. The brush was annealed under vacuum at 160 °C (2.6×10^3 Pa) for 5 h to ensure all solvent was removed. A scheme of the reaction is available in Scheme S1 of the supporting information.

2.5. Characterization of PMMA brush thicknesses and homogeneity

Film thickness of the initiator substrates and subsequent PMMA thin films was measured by ellipsometry using a J.A. Woolam spectroscopic ellipsometer M2000 with variable wavelength scans from 200 nm to 1000 nm at angles of 65°, 70°, and 75°. All ellipsometric thickness measurements were performed in a 1.5 cm × 1.5 cm grid, consisting of 80 measurement points to determine the macroscopic thickness variability of the brush substrates. The ellipsometric thicknesses were determined from the average of all grid points with the error representing one standard deviation of the data. Surface morphology and RMS roughness was determined using a Bruker Dimension Icon atomic force microscope (AFM) using ScanAsyst-Air probes with a nominal spring constant of 0.4 N/m. For each film, AFM measurements were performed on at least separate three locations and the error reported with all measurements represents one standard deviation. Thickness characterization of the dry films was conducted using both ellipsometry and XRR in order to investigate the macroscopic heterogeneity of the films, ensuring that the XRR measurements thickness and roughness measurements were representative of the microscopic structure of the film.

2.6. XRR of dry and swollen brushes

All XRR measurements were performed using a Phillips X'PERT X-ray diffractometer with a Cu K_α source (1.5412 Å, wavelength divergence of 3×10^{-3} Å, angular divergence of 3×10^{-5} rad). The X-rays were focused using a curved mirror into a quadruple bounce Ge [220] crystal monochromator. The specular condition was

obtained for the reflected beam using a triple bounce Ge [220] crystal monochromator. The scattering vector was calculated from:

$$Q = \frac{4\pi \sin \theta}{\lambda} \qquad (3)$$

where θ is the incident angle and λ is the wavelength of the X-ray beam. Specular reflection was collected with incident angle starting from 0.1° to 1.5° for the thin film and 0.1°–0.8° for the thick film as additional fringes were not discernable due to surface roughness for the thicker film at higher angles of incidence.

Vapor swelling experiments were performed at 25 °C using an aluminum chamber sealed over the sample platform with X-ray transparent beryllium windows. A solvent reservoir (5 mL) was left at the base of the chamber and the solvent vapor was permitted to saturate the chamber for 16 h prior to measurement. This protocol was used to ensure the chamber was saturated with vapor before measurement regardless of the vapor pressure of the solvent at atmospheric pressure and temperature; periodic rapid scans were taken to verify that the brush reached maximum swelling at the 16 h limit. XRR scans were performed at 0.003° steps with a 10 s scan time at each step. After measurement, the wafer was vacuum annealed in a vacuum oven at 160 °C for 5 h to ensure the brush was free of solvent prior to next scan. Both poor solvents (methanol, hexane, cyclohexane) and good solvents (acetone, ethyl acetate, tetrahydrofuran, and toluene) were used to swell both films. These solvents were chosen due to the large change in solvent quality ($0.43 \leq \chi \leq 1.8$) for PMMA and sufficiently high vapor pressure to saturate the chamber.

Data reduction for each reflectivity curve was done using a MATLAB routine that consisted of footprint correction, conversion of the scattering angle into scattering vector and normalization of the scattering intensity. Theoretical reflectivity curves were modeled using NIST Reflfit software [39], which uses Parratt's formalism for given layer thickness and scattering length densities. Fitting the model to experimental data yielded film thickness, scattering length density, roughness, and linear absorption coefficient, the quality of fit was indicated by Pearson's chi-squared test. Initial predictions of scattering length density (SLD) for PMMA, solvents, bulk silicon were calculated from the NIST NCNR website [40] and SLD values of native SiO_2 films on commercially-available wafers were obtained from the literature and compare well to XRR curves of cleaned silicon wafers in the laboratory [41]. Values for SLDs are provided in Table S1 of the supporting information. The thickness and scattering length density (SLD) of the dry brushes were measured prior to each swelling experiment. The XRR reflectivity curves and model curve fits for the polymer brush layers are shown in Fig. S1a and S1b of the supporting information and the SLD and thickness values are summarized in Table S2 in supporting information. The high reproducibility of the reflectivity curves for the dry measurements for both the thick and thin brush indicates that solvent was completely removed from the films during

vacuum annealing before the next solvent was added and that degradation of the film was not observed [42]. Fig. S2 of the supporting information contains SLD profiles indicating the consistency of the instrument (Fig. S2a) and the experimental (Fig. S2b) measurement.

3. Results and discussion

3.1. Characterization of the dry PMMA brushes

PMMA brushes were synthesized from the initiator substrates to create two comparable polymer brush regimes: a thin polymer brush (h_o = 12.6 nm ± 0.5 nm), and a thicker one (h_o = 71.4 nm ± 1.0 nm) in order to compare this method of grafting density measurement on two length scales. Brush homogeneity is critical to accurate brush measurements in XRR, as the measured thickness and scattering length densities are an average of the area of the film in the X-ray beam path. Therefore, AFM height images of the brushes (Fig. 1b and c) were taken to demonstrate that surface coverage of the brushes were homogeneous, and well-controlled on the microscale.

The thick and thin films had RMS roughnesses (R_q) of 0.4 nm and 2.0 nm, respectively, after thermal annealing. The macroscopic homogeneity of the films was measured using ellipsometric mapping (Fig. S3 of the supporting information) and average thicknesses agrees well with dry thicknesses measured by XRR with a standard deviation of less than 1 nm for both thin and thick brushes.

As an initial estimate of grafting density, solution polymer resulting from sacrificial initiator was recovered for both brushes and characterized by gel permeation chromatography. The number average molecular mass (M_n) values were used in equation (2) to calculate grafting density using the bulk density of PMMA, as the measured SLD of the brushes is within 2% of theoretical SLD of bulk PMMA. The M_n and σ results are shown in Table 1. The estimated grafting densities are 0.225 chains/nm^2 and 0.311 chains/nm^2 for the thin and thick brushes, respectively. Since both brushes were synthesized from identical initiator substrates, we expected σ for both brushes to be approximately equal. The 32% disparity indicates that using solution polymer to estimate M_n in equation (2) will result in an inaccurate calculation of grafting density.

3.2. Swelling behavior of PMMA brushes

The XRR curves of the thin and thick PMMA brushes are presented in Fig. 2a and b respectively. Thickness and SLD measurements of the dry state of the PMMA brushes are shown in Table S3 of the supporting information. After equilibration in saturated solvent vapor, XRR curves for the swollen brushes were collected and modeled as a single layer with a uniform density. This single layer model yielded poor fits to the XRR curves, especially at Q values above 0.05 Å^{-1}. Specifically, treating the brushes as a single

Table 1
Summary of Polymer Brush molecular mass and grafting density approximated from sacrificial initiator PMMA.

PMMA brush	M_n from solution PMMA (g/mol)	[b]M_w/M_n	[a]σ (chains/nm^2)
Thin	38,100	1.2	0.225 ± 0.008
Thick	151,000	1.6	0.311 ± 0.002

[a] Grafting density calculated using equation (2), where M_n is of free polymer in solution.
[b] M_w/M_n is the polydispersity index, calculated from the weight average molecular mass (M_w) and M_n.

layer caused a premature decay of the oscillation in the fit curve at larger scan angles, when distinct fringes were present in the raw data. To improve the fits, we modified the reflectivity model by treating the film as a multi-layered film where each layer has a unique scattering length density. No discernable improvement in the fit was observed with additional layers beyond three layers. An example of this multi-layer procedure for fitting of the swollen brush is shown in Fig. S4 of the supporting information, using the thick brush swollen in toluene as a representative depiction of the resulting fit. Fig. 2a and b are the reflectivity curves of the thin and thick brush swollen the various solvents, respectively. Also included in the figures are fits to the reflectivity curves using the three-layer model. For both brushes, a decrease in the critical angle is observed as solvent quality increases, indicating a decrease in polymer concentration of the brush. Solvent quality is categorized by the solvent–polymer interaction parameter, χ, between the particular solvent and the PMMA brush. The solvent is considered a good solvent when $\chi \leq 0.5$, whereas the solvent is indicative of a poor solvent when $\chi \geq 0.5$. Both non-polar and polar solvents were used for good and poor solvents to see if polarity differences had an impact on swelling trends. A shift in the fringes to lower Q values is also observed, as highlighted by the dashed line in Fig. 2a and b. This change denotes that the brush thicknesses increase as expected with quality of solvent as the chains extend away from the surface.

The SLD profiles for the PMMA brushes in each solvent are shown in Fig. S5b through S5h of the supporting information and a visualization of the PMMA brush swelling in good versus poor solvents is depicted in Scheme 1. Regardless of whether the PMMA is swollen in a good or bad solvent, we represent the brush density with a three-layer model. In each case, layers 1, 2 and 3 represent the polymer chain ends tethered to the substrate, the middle portion of the chain, and the chain ends exposed to the environment, respectively.

For good solvents, the SLD of the film decreases as thickness increases for the thin brushes, where the SLD of all 3 layers is less than that of the dry brush. This is another indication of swelling, consistent with the thickness measurement, as solvent SLDs in this experiment are always less than they dry polymer SLD. For the poor solvent systems, the layer 2 shows an SLD as high as, or slightly higher than, dry PMMA, indicative of collapsed chains. We find that the SLD is much lower near the surface than dry film SLD (layer 1 in Scheme 1), which would indicate the presence of a thin solvent-rich layer. Additionally, we note that the trends in SLD profiles for each poor solvent are consistent between the thin and thick polymer brushes.

Solvent-rich "depletion" layers near the substrate of a polymer thin film have been predicted in simulations [43,44] and observed experimentally [34,45,46] A larger depletion layer is observed for methanol swelling and we speculate that methanol is diffusing through the film and preferentially adsorbing to the exposed SiO$_2$ surface, as observed previously [47]. There is a smaller depletion layer for hexane and cyclohexane, and it is most likely a result of swelling of the eleven-carbon initiator with the hydrophobic solvents. Layer 3 describes the chain ends of the polymer brush that is farthest away from the substrate. This region can be affected by chain length distributions, macroscopic roughness, such as defects at the surface, or buried chain ends, which would not be easily observed in the middle layer, but would show as a lower density of chains near the end of the brush.

3.3. Determination of 1D swelling of polymer brushes

The dimensionality of swelling can be determined from the brush swelling results by comparing the total thickness swelling
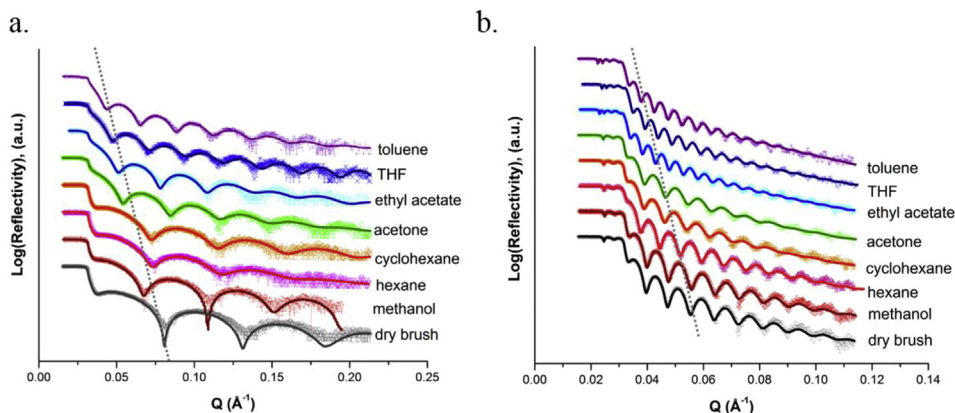
Fig. 2. XRR data (points) with model fits (solid lines) for PMMA brushes swollen with various solvent vapors: (a) 12 nm brush (thin) and (b) 68 nm brush (thick). Each curve is offset by one (b) or two (a) decades for clarity. The dashed line is meant to guide the eye.

ratio to the volumetric swelling ratio. This assessment has been previously demonstrated in the vapor swelling of crosslinked polyamide films using XRR [48] and ellipsometry measurements [49]. The comparison between thickness and volumetric swelling allows for a preliminary qualitative determination of the grafting density regime of the brush. If the grafted chains are in the low grafting density regime (reduced tethering density, $\Sigma \approx 5$, where $\Sigma = \sigma \pi R_g^2$) [34], there will be more lateral swelling, relative to thickness swelling. Brushes in the moderate to high grafting density regimes ($\Sigma \geq 12$) swell only normal to the grafted surface. The thickness swelling ratio, α, is defined:

$$\alpha = \frac{h_s}{h_d} \quad (4)$$

where h_s is the thickness of the swollen brush, and h_d is the thickness of the dry, annealed brush. The change in SLD can be correlated to polymer volume fraction, ϕ, using: [50]

$$\phi = \frac{Q_c^2 - Q_{c,s}^2}{Q_{c,0}^2 - Q_{c,s}^2} \quad (5)$$

where Q_c^2, $Q_{c,0}^2$, and $Q_{c,s}^2$ are the scattering length densities of the swollen brush, the dry brush, and the solvent, respectively. To determine the overall ϕ of the brushes based on the three-layer reflectivity model, a weighted average was used:

$$\phi \equiv \phi_{p,avg} = \frac{h_1 \phi_{p,1} + h_2 \phi_{p,2} + h_3 \phi_{p,3}}{h_{tot}} \quad (6)$$

where h_x is the thickness of the sub-layer ($x = 1$, 2, or 3) of the total thickness (h_{tot}).

The volumetric swelling ratio (S) is the inverse of the polymer brush volume fraction, and the relationship between S and α is: [48]

$$S = \frac{1}{\phi} \quad (7)$$

$$\phi = \frac{1}{\alpha^n} \quad (8)$$

where n is the dimensionality of swelling; $n = 1$ for swelling along the thickness direction and $n = 3$ for isotropic swelling. The swelling ratio is depicted in Fig. 3, with the slopes and quality of fits (R^2) summarized in Table 2. For the thick brush, the slope of the line is $n = 0.9$ regardless of if a one- or three-layer model is used. For the thin brush, however, the films have poor correlation with volumetric swelling when using a one-layer model. When accounting for SLD changes throughout the film using the three-layer model, the thin films demonstrate one dimensional swelling as well. Since both films swell only along the thickness direction, their behavior in identical solvents can be used to compare thermodynamics within the brushes.
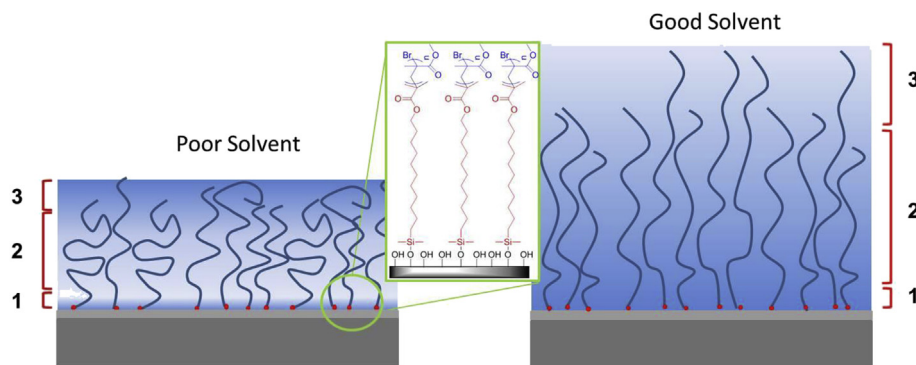
Scheme 1. Depiction of brush swelling in poor (methanol, hexane, and cyclohexane) and good (ethyl acetate, acetone, tetrahydrofuran, and toluene) quality solvent vapor. The three regimes depict substrate effects (1), bulk swelling of the brush (2) and decreased polymer density due to chain ends (3) for both poor and good solvents. The position of the 3 regions is defined by the best fit location of the layer interfaces in the XRR model; the locations shown here qualitatively approximate the typical case for each solvent group.
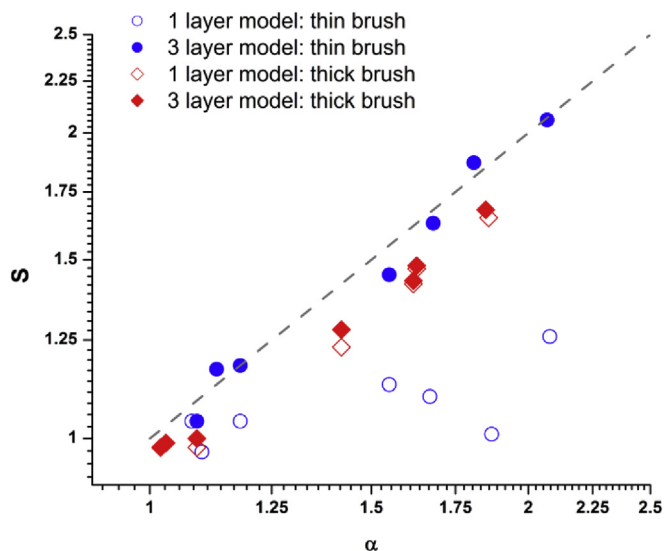
Fig. 3. Volumetric (S) versus linear swelling ratio (α) for a both thin (blue) and thick (red) PMMA brushes fit with a one-layer model (open symbols) and a three-layer (closed symbol) model. The dashed line (n = 1) is the S = α line representing ideal one-dimensional swelling. (For interpretation of the references to colour in this figure legend, the reader is referred to the web version of this article.)

3.4. Thermodynamics of polymer brush swelling

Using a modified Flory−Huggins theory, the free energy of the brush upon swelling can be separated into energy contributions for the mixing (ΔF_{mix}) and elastic (ΔF_{el}) components,

$$\Delta F = \Delta F_{mix} + \Delta F_{el} \qquad (9)$$

Differentiating the free energy with respect to moles of solvent yields a change in chemical potential of the brush (μ_s) described by Birshtein et al. [51]

$$\frac{\Delta \mu_s}{RT} = ln(a_s) = \ln(1 - \phi) + \phi + \chi\phi^2 + \frac{3\sigma^2 a^4}{\phi} = 0 \qquad (10)$$

The first three terms in equation (10) are derived from Flory−Huggins free energy of mixing, while the last term is the elastic energy due to Gaussian stretching of the chains, assuming the chain segments are uniformly distributed in the thickness direction. Assuming a solvent activity ≈ 1 for saturated vapor, equation (10) reduces to an expression that can be used to solve for grafting density (σ) provided that the polymer volume fraction (φ) and polymer solvent interaction parameter (χ) are known. Theoretical derivations of brush grafting density often describe grafting density as a dimensionless quantity, normalized by the area of a monomer unit. For clarity, all equations are reported in dimensional grafting density and the area of a monomer unit was estimated at $a^2 = 0.57$ nm², based on the dry film density of PMMA brushes measured in XRR, derived in the supporting information (equation S(1)).

Table 2
Swelling dimension determinations for 1 layer and 3 layer models of brushes from Fig. 3. R^2 is the coefficient of determination, indicating the quality of the linear fit.

PMMA brush	Model	n	R^2
Thin	1 layer	0.22	0.453
	3 layer	1.00	0.976
Thick	1 layer	0.87	0.982
	3 layer	0.90	0.992

In our experiments, the aim was to avoid any anomalies at low activities, such as excess solvent uptake [6], by measuring different solvents at maximum brush swelling for a given solvent. A plot of α versus χ for the thick and thin brushes (Fig. 4, values listed in Table S3 of the supporting information) was fit to equation (10), using equations (7) and (8) to convert α to φ, in order to determine the grafting density of the thick and thin PMMA brushes. The data in Fig. 4 appears to be grouped by overall solvent quality. The poor solvents for both brushes are tightly grouped at low swelling ratios and large χ parameters, while there is a large change in swelling ratios for the good solvents, all with literature χ values ≈ 0.45 [52]. The fit of equation (10) to the data yield grafting densities for the thin and thick brushes of σ_thin = 0.24 chains/nm² and σ_thick = 0.35 chains/nm², respectively. While the values of σ are comparable to the estimation of σ from equation (2), the overall fit in both brushes is poor and the grafting density between the thin and thick brushes are inconsistent. These results indicate that the Birshtein model in its current form does not accurately describe this swelling experiment.

The Birshtein model makes two fundamental assumptions: 1) the grafting density is not too high (σa << N^{2/3}), and 2) the solvent−interaction parameter is known. We can rearrange equation (10) to calculate χ as a function of φ and σ (equation S2 in supporting information), using the estimated σ values from Table 1. The values of χ calculated in this fashion are provided in Table 3, along with χ values reported in the literature [52]. The calculated χ for thin brush swollen in methanol and hexane are higher than the literature values, and χ for the thick brush is higher still. The differences in χ between acetone, ethyl acetate, tetrahydrofuran, and toluene are very small in the literature (Δχ ≤ 0.03), but are much larger in both the thin and thick PMMA brushes. The polymer solvent interaction parameter for each solvent is also inconsistent between thick and thin brushes; with the exception of acetone, the literature χ for a given good solvent has no discernible trend in the relationship to the calculated χ. A portion of this inconsistency could be due to the intrinsic error from our assumption in Table 1 that free and tethered chains have the same molecular weight distribution. However, the lack of fit is independent of the precise value of σ, so this source of error cannot account for the entire difference in trend between literature and calculated χ values.
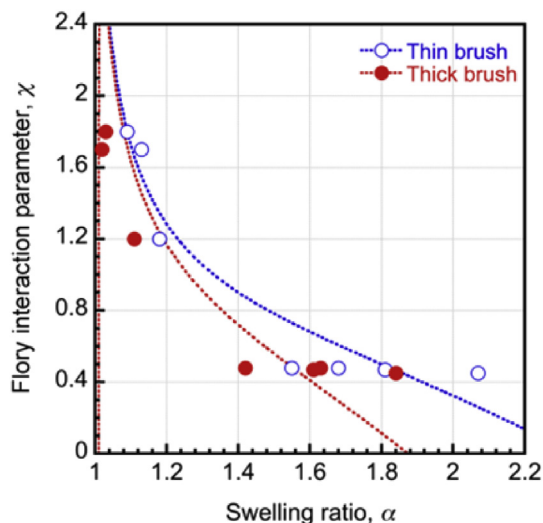

Fig. 4. Modeling grafting density using literature chi values.

Table 3
Comparison of polymer–solvent interaction parameter values calculated from estimated grafting density.

Solvent	Literature χ (solution)	Calculated χ (vapor)	
		Thin brush	Thick brush
Methanol	1.2	1.38	1.77
Hexane	1.8	1.81	2.54
Acetone	0.48	0.76	0.76
Ethyl acetate	0.48	0.64	0.50
Tetrahydrofuran	0.47	0.39	0.49
Toluene	0.45	0.32	0.20

This result indicates that there are additional interactions affecting brush solvation beyond concentration or thickness dependence, as the differences in χ between thin and thick brushes would be proportional if χ were dependent on ϕ. We could, in principle, approach these deviations in terms of binary and ternary interactions using derivations for the free energy of mixing in earlier work by Zhulina and Birshtein including expressions for the second and third virial coefficients [17]. Unfortunately, the measurements of virial coefficients in brushes and thin films are non-trivial and beyond the scope of this work. These challenges in accurately quantifying χ within polymer brushes presently prevent us from concluding if the mean field theory of Birshtein in polymer brush swelling is an accurate description of experimental swelling.

The χ parameter in polymer brushes is unknown due to contributions of concentration, confinement, and conformation on solvent quality. There are several ways to determine the quality of bulk polymer/solvent interactions using membrane osmometry, vapor sorption measurements, or inverse gas chromatography (iGC), for different concentration regimes, listed here from least to most concentrated, where iGC works for polymer volume fractions (ϕ) approaching 1 [53]. These methods can yield very different polymer–solvent interaction parameters due to the influence of concentration on that interaction parameter, and the existence of higher order interactions (such as third virial coefficients) where polymer chains self-interact, whether due to inter-chain or intra-chain interaction. Vapor swelling has been used to determine χ for the polymer–solvent and polymer–polymer interactions recently in conjugated [54] and crosslinked [55] polymer thin films, where overall chain solubility is poor. Recent experiments by Wagman et al. evaluate swelling in monolayers of bio-macromolecules in water vapor, modifying existing Flory theory to include ternary interactions between polymer, water, and vacant sites [56]. In swelling a brush with vapor, special consideration must also be paid to the polymer–solvent–gas interface not only along the extended chains, but at the chain ends as well [57]. Vapor phase swelling, even in good solvents yields step-like density profiles rather than the parabolic profiles observed in solution swelling in the strong stretching regime [34], as was also observed in this study. Swelling between saturated vapor and liquid should be identical from a thermodynamic perspective, as the chemical potential in both systems are equal. A similar observation has been discussed in the membrane and elastomer community, known as Schroeder's paradox [58]; swelling of membranes in liquid yields larger mass uptake than swelling in saturated vapor even after equilibration for long periods of time. This observation must be further explored for brushes to quantify the differences between vapor and liquid solvation of the polymer brush.

The effects of confinement in very thin polymer films, less than 100 nm in dry thickness, exhibit thickness-dependent swelling, as surface interactions and reduced mobility affect the solvent–polymer interaction [59,60]. Determination of χ through gravimetric methods on thin films is generally conducted on films several hundred nanometers thick to determine the bulk polymer solvent interaction deconvoluted from substrate and surface effects [61]. While attractive and repulsive surface interactions in brushes have been studied [45], the impact of surface effects cannot be decoupled from brush grafting density as the overlap and extension of chains at higher grafting density can mitigate an attractive surface.

Finally, the effect of extended conformation of polymer brush chains must be considered in the solvent–polymer interaction parameter. Molecular structure simulations conducted by Baulin and Halperin indicate monomer concentration dependence on χ for thermoresponsive polymer brushes due to decreasing polymer volume fraction as the chains stretch away from the substrate [62]. Brush swelling experiments combined with surface stress measurements by Gutmann and coworkers indicate that free surface energy resulting from interfacial tension between solvent and brush significantly adds to the enthalpic and entropic energy contributions to χ yielding more favorable mixing between elongated polymer brush chains and solvents than solution χ values would predict [33]. This is contradictory to vapor sorption studies in polymer brushes [34] and polymer films [63], where the dominance on the entropic contribution to χ makes its value much higher than predicted Hildebrand solubility parameters. There are several theoretical studies on the impact of molecular structure, entropic considerations, and ternary interactions that can impact the Flory–Huggins interaction parameter [64–66]; however, these theories must be tested using experimental results to determine limits of theory and develop better measurements to quantify brush thermodynamics.

4. Conclusions

A measurement to quantify swelling of polymer brushes using saturated solvent vapor has been established as a preliminary study of solvent–polymer brush thermodynamics. Grafting density calculations from experimental changes in polymer volume fraction are currently unreliable because the χ parameter for a particular solvent–polymer brush system is unknown due to changes in the concentration, confinement, and conformation with solvent quality. This manuscript is a preliminary effort towards accurately quantifying chain grafting density. Further studies to expand understanding of thermodynamics of polymer brushes should include a systematic comparison of polymer solvation within a thin film, including incorporation of higher order virial coefficients as a more absolute way to describe solvent quality, comparison of solvation between liquid and vapor swollen systems, and contributions from monomer structure on the thermodynamics of the chains. Expansion of mean field and self-consistent field calculations should also be made to model the differences between vapor and solvent swelling. In addition to establishing better measures of grafting density in the brush regime, quantifying thermodynamics of grafted polymer layers will expand the understanding of polymer thin films across several grafting density regimes, towards a universal expression where contributions of solvent, grafting density, surface energetics, and molecular mass can be enumerated. As more knowledge on thermodynamics and kinetics of polymer brushes becomes known, the potential of polymer brushes as a tool to develop controllable membranes, chromatographic stationary phases, and tunable sensors will continue to expand.

Appendix A. Supplementary data

Supplementary data related to this article can be found at http://dx.doi.org/10.1016/j.polymer.2015.05.030.

References

[1] Toomey R, Tirrell M. Annu Rev Phys Chem 2008;59:493–517.
[2] Minko S. J Macromol Sci C Polym Rev 2006;46(4):397–420.
[3] Advincula R, Brittain WJ, Caster KC, Rühe J, editors. Polymer Brushes: Synthesis, Characterization, Applications. Weinheim, Germany: Wiley-VCH Verlag BmbH & Co. KGaA; 2004.
[4] Milner ST. Science 1991;251(4996):905–14.
[5] Bliznyuk V, Galabura Y, Burtovyy R, Karagani P, Lavrik N, Luzinov I. Phys Chem Chem Phys 2014;16(5):1977–86.
[6] Laschitsch A, Bouchard C, Habicht J, Schimmel M, Rühe J, Johannsmann D. Macromolecules 1999;32(4):1244–51.
[7] Liao W-P, Elliott IG, Faller R, Kuhl TL. Soft Matter 2013;9(24):5753.
[8] Brittain WJ, Minko S. J Polym Sci A Polym Chem 2007;45(16):3505–12.
[9] Azzaroni O. J Polym Sci A Polym Chem 2012;50(16):3225–58.
[10] Ayres N. Polym Chem 2010;1(6):769.
[11] Jain P, Baker GL, Bruening ML. Annu Rev Anal Chem Palo Alto Calif 2009;2: 387–408.
[12] Chen T, Ferris R, Zhang J, Ducker R, Zauscher S. Prog Polym Sci 2010;35(1–2): 94–112.
[13] Zhao B, Brittain W. Prog Polym Sci 2000;25(5):677–710.
[14] Wu T, Efimenko K, Genzer J. J Am Chem Soc 2002;124(32):9394–5.
[15] De Gennes PG. Macromolecules 1980;13(5):1069–75.
[16] Milner ST, Witten TA, Cates ME. Macromolecules 1988;21(8):2610–9.
[17] Zhulina YB, Borisov OV, Pryamitsyn VA, Birshtein TM. Macromolecules 1991;24(1):140–9.
[18] Moh LCH, Losego MD, Braun PV. Langmuir 2011;27(7):3698–702.
[19] Wu T, Efimenko K, Vlcek P, Šubr V, Genzer J. Macromolecules 2003;36(7): 2448–53.
[20] Tomlinson MR, Genzer J. Macromolecules 2003;36(10):3449–51.
[21] Milner ST, Witten TA, Cates ME. Europhys Lett 1988;5(5):413–8.
[22] Edmondson S, Osborne VL, Huck WTS. Chem Soc Rev 2004;33(1):14–22.
[23] Koylu D, Carter KR. Macromolecules 2009;42(22):8655–60.
[24] Devaux C, Chapel JP, Beyou E, Chaumont P. Eur Phys J E 2002;7(4):345–52.
[25] Husseman M, Malmström EE, McNamara M, Mate M, Mecerreyes D, Benoit DG, et al. Macromolecules 1999;32(5):1424–31.
[26] Pasetto P, Blas H, Audouin F, Boissiere C, Sanchez C, Save M, et al. Macromolecules 2009;42(16):5983–95.
[27] Kang C, Crockett RM, Spencer ND. Macromolecules 2014;47(1):269–75.
[28] Turgman-Cohen S, Genzer J. Macromolecules 2010;43(22):9567–77.
[29] Turgman-Cohen S, Genzer J. J Am Chem Soc 2011;133(44):17567–9.
[30] Biesalski M, Rühe J. Langmuir 2000;16(4):1943–50.
[31] Habicht J, Schmidt M, Rühe J, Johannsmann D. Langmuir 1999;15(7):2460–5.
[32] Domack A, Prucker O, Rühe J, Johannsmann D. Phys Rev E 1997;56(1): 680–9.
[33] Lenz S, Rühm A, Major J, Berger R, Gutmann JS. Macromolecules 2011;44(2): 360–7.
[34] Galvin CJ, Dimitriou MD, Satija SK, Genzer J. J Am Chem Soc 2014;136(36): 12737–45.
[35] Matyjaszewski K, Miller PJ, Shukla N, Immaraporn B, Gelman A, Luokala BB, et al. Macromolecules 1999;32(26):8716–24.
[36] Li C, Benicewicz BC. Macromolecules 2005;38(14):5929–36.
[37] Ramakrishnan A, Dhamodharan R, Rühe J. Macromol Rapid Commun 2002;23(10–11):612.
[38] Gorman CB, Petrie RJ, Genzer J. Macromolecules 2008;41(13):4856–65.
[39] Kienzle PA, O'Donovan KV, Ankner JF, Berk NF, Majkrzak CF. Reflpak.
[40] Kienzle PA. Neutron activation calculator http://www.ncnr.nist.gov/resources/activation/ [accessed 09.04.14].
[41] Nelson A. J Appl Crystallogr 2006;39(2):273–6.
[42] Brown HR, Char K, Deline VR. Macromolecules 1990;23(13):3383–5.
[43] De Vos WM, Leermakers FAM. Polym Guildf 2009;50(1):305–16.
[44] Perahia D, Wiesler DG, Satija SK, Fetters LJ, Sinha SK, Milner ST. Phys Rev Lett 1994;72(1):100–3.
[45] Karim A, Satija SK, Douglas JF, Ankner J, Fetters LJ. Phys Rev Lett 1994;73(25): 3407–10.
[46] Vogt BD, Soles CL, Lee H-J, Lin EK, Wu W. Langmuir 2004;20(4):1453–8.
[47] Gallagher PD, Satija SK, Karim A, Douglas JF, Fetters LJ. J Polym Sci B Polym Phys 2004;42(22):4126–31.
[48] Chan EP, Young AP, Lee J-H, Chung JY, Stafford CM. J Polym Sci B Polym Phys 2013;51(6):385–91.
[49] Toomey R, Freidank D, Rühe J. Macromolecules 2004;37(3):882–7.
[50] Vogt BD, Lee H-J, Prabhu VM, DeLongchamp DM, Lin EK, Wu W, et al. J Appl Phys 2005;97(11):114509.
[51] Birshtein TM, Lyatskaya YV. Macromolecules 1994;27(5):1256–66.
[52] Mark JE, editor. Physical properties of polymers handbook. New York: New York, NY: Springer; 2007.
[53] Errede LA. J Appl Polym Sci 1992;45(4):619–31.
[54] Emerson JA, Toolan DTW, Howse JR, Furst EM, Epps TH. Macromolecules 2013;46(16):6533–40.
[55] Manoli K, Goustouridis D, Raptis I, Valamontes E, Sanopoulou M. J Appl Polym Sci 2010;116(1):184–90.
[56] Wagman M, Medalion S, Rabin Y. Macromolecules 2012;45(23):9517–21.
[57] Cohen Stuart MA, de Vos WM, Leermakers FAM. Langmuir 2006;22(4): 1722–8.
[58] Vallieres C, Winkelmann D, Roizard D, Favre E, Scharfer P, Kind M. J Memb Sci 2006;278(1–2):357–64.
[59] Mattsson J, Forrest J, Börjesson L. Phys Rev E 2000;62(4):5187–200.
[60] Fryer DS, Peters RD, Kim EJ, Tomaszewski JE, de Pablo JJ, Nealey PF, et al. Macromolecules 2001;34(16):5627–34.
[61] Manoli K, Goustouridis D, Chatzandroulis S, Raptis I, Valamontes ES, Sanopoulou M. Polym Guildf 2006;47(17):6117–22.
[62] Baulin VA, Halperin A. Macromol Theory Simul 2003;12(8):549–59.
[63] Read DH, Martin JE. Anal Chem 2010;82(12):5373–9.
[64] Dudowicz J, Freed KF, Douglas JF. J Chem Phys 2002;116(22):9983.
[65] Douglas JF, Dudowicz J, Freed KF. J Chem Phys 2007;127(22):224901.
[66] Egorov SA. J Chem Phys 2008;129(6):064901.